Nuclear Factor I X Deficiency Causes Brain Malformation and Severe Skeletal Defects[▽]

Katrin Driller,[1] Axel Pagenstecher,[2]† Markus Uhl,[3] Heymut Omran,[4] Ansgar Berlis,[5] Albert Gründer,[1]‡ and Albrecht E. Sippel[1]*

Institut für Biologie III, Fakultät für Biologie,[1] and Abteilung Neuropathologie,[2] Albert-Ludwigs Universität Freiburg, Röntgendiagnostik, Radiologische-Universitätsklinik,[3] Department of Pediatrics and Adolescent Medicine, University Hospital,[4] and Neuroradiologie, Neurozentrum,[5] Freiburg, Germany

The transcription factor family of nuclear factor I (NFI) proteins is encoded by four closely related genes: *Nfia*, *Nfib*, *Nfic*, and *Nfix*. A potential role for NFI proteins in regulating developmental processes has been implicated by their specific expression pattern during embryonic development and by analysis of NFI-deficient mice. It was shown that loss of NFIA results in hydrocephalus and agenesis of the corpus callosum and that NFIB deficiency leads to neurological defects and to severe lung hypoplasia, whereas *Nfic* knockout mice exhibit specific tooth defects. Here we report the knockout analysis of the fourth and last member of this gene family, *Nfix*. Loss of NFIX is postnatally lethal and leads to hydrocephalus and to a partial agenesis of the corpus callosum. Furthermore, NFIX-deficient mice develop a deformation of the spine, which is due to a delay in ossification of vertebral bodies and a progressive degeneration of intervertebral disks. Impaired endochondral ossification and decreased mineralization were also observed in femoral sections of *Nfix*$^{-/-}$ mice. Consistent with the defects in bone ossification we could show that the expression level of tetranectin, a plasminogen-binding protein involved in mineralization, is specifically downregulated in bones of NFIX-deficient mice.

Nuclear factor one (NFI) proteins were identified in 1982 as site-specific DNA-binding proteins binding to regulatory elements of the chicken lysozyme gene (50). Later studies revealed that these proteins function as transcriptional activators and repressors of cellular and viral genes but are also involved as cellular host factors in viral replication (27). In vertebrates, the *Nfi* gene family consists of four closely related genes, named *Nfia*, *Nfib*, *Nfic*, and *Nfix* (37, 58). They encode proteins with a conserved N-terminal DNA-binding and dimerization domain (26) and a C-terminal transactivation/repression domain which exhibits a high variability due to extensive alternative splicing (29, 38, 48). NFI family members act as homo- and heterodimers (39) and bind with high affinity to the palindromic consensus sequence 5′-PyTGGCA-N_3-TGCCAPu-3′ (6, 20, 51). Besides the original detection of binding sites for NFI proteins in regulatory regions of the lysozyme gene (6, 50), NFI-binding motifs were subsequently detected in promoters of genes expressed in almost every organ, including brain (4, 32, 36), lung (2), liver (33), intestine (69), muscle (61), and connective tissue and skeletal elements (1, 12, 52, 53, 64).

In order to gain insight into the individual and common functions of the murine *Nfi* genes, knockout analyses of each family member have been undertaken. Loss of NFIA is perinatally lethal and results in hydrocephalus, corpus callosum agenesis, and defects in midline glial structures (15, 59). NFIB-deficient mice die at birth of respiratory failure due to an arrest in late lung development and also show neuronal defects that are similar, but more severe, than in *Nfia*$^{-/-}$ mice (28, 63). Disruption of the murine *Nfic* gene leads to a lack of molar roots as well as thin and brittle mandibular incisors. Besides these tooth pathologies, no other defects are observed, and when fed soft chow, *Nfic*$^{-/-}$ mice have a normal life span (62). This, and the stringent spatiotemporal gene regulation of NFI family members during embryogenesis and in adult animals, shows that NFI proteins exert important functions during mouse development (11).

Here we report for the first time the inactivation of the *Nfix* gene in the mouse, by inserting a *lacZ* reporter gene into the reading frame of exon 2, thereby deleting the essential coding region of the DNA-binding domain. *Nfix*$^{-/-}$ mice are growth retarded and die between postnatal day 21 (P21) and P28. They exhibit an enlargement of the lateral and third brain ventricles and a partial agenesis of the corpus callosum. Additionally, NFIX-deficient mice show a kyphotic deformation of the spine and impaired endochondral ossification in the vertebrae and femur. The expression of tetranectin, a protein involved in bone metabolism, has been found to be downregulated in *Nfix*$^{-/-}$ mice. Taken together, our studies provide evidence that NFIX plays an essential role in the development of the brain and the skeleton.

MATERIALS AND METHODS

Targeting vector. A murine λ FIX II library (Stratagene) generated from Black Agouti 129 genomic DNA (57) was screened with an *Nfix* cDNA probe for clones containing exon 2. The isolated clones were characterized, and the localization of exon 2 was confirmed by restriction mapping, Southern blot analysis, and DNA sequencing. For the construction of the targeting vector, a 7.6-kb exon 2-containing ApaI fragment was used. Using site-directed mutagenesis, an EcoRI site

* Corresponding author. Mailing address: Albert-Ludwigs Universität, Institut für Biologie III/Genetik, Schänzlestr. 1, D-79104 Freiburg, Germany. Phone: 49-761-2032760. Fax: 49-761-2032745. E-mail: sippel@biologie.uni-freiburg.de.

† Present address: Abteilung Neuropathologie, Universität Marburg, Marburg, Germany.

‡ Present address: Max-Planck-Institut für Immunologie, Freiburg, Germany.

▽ Published ahead of print on 12 March 2007.

was generated at the 5′ end of exon 2, thereby deleting the entire 3′ region and 32 bp of the following intron. This EcoRI site was then used to integrate a cassette containing the bacterial β-galactosidase gene (β-Gal) and a loxP-flanked neomycin phosphotransferase gene (neo^r), driven by the herpes simplex virus thymidine kinase (HSV-tk) promoter, into the reading frame of exon 2, resulting in a fusion of the first 4 nucleotides of exon 2 and β-Gal. The β-Gal-pA and pHSV-tk-loxP-neo^r-loxP cassette replaces 564 bp of *Nfix*, including all but 4 bp of exon 2. It is flanked by a 5.1-kb homology arm at the 5′ end and 2 kb at the 3′ end. In order to place an HSV-tk cassette as negative selection marker at each end of the vector, the construct was cloned into the BamHI site of the λKO vector (49).

Gene targeting. CJ7 embryonic stem (ES) cells (1×10^7) were electroporated with 25 μg of NotI-linearized targeting vector, plated on embryonic feeder cells on tissue culture dishes, and then selected in 0.35 mg/ml G418 (Gibco-BRL) and 2 μM ganciclovir (Sigma). After 5 to 7 days of selection, distinct colonies were picked and expanded in 96-well plates. Two plates were frozen, and one plate was used for DNA isolation. Southern blot analysis of EcoRV-digested genomic DNA revealed 5 out of 178 clones positive for homologous recombination, corresponding to a recombination efficiency of 2.8%.

Cre-mediated neo^r deletion. To delete the neo^r selection marker, 1×10^7 targeted ES cells from two independent *Nfix*$^{lacZ\text{-}neor}$ ES cell clones were transfected with 30 μg of supercoiled Cre-encoding plasmid (pPGK cre bpA) by electroporation. Cells were plated on 9-cm dishes for 24 h and then replated at 1×10^3 cells/9-cm plate. Four days after replating, 48 distinct colonies were picked and plated on one 96-well selection plate and one duplicate plate. As soon as colonies became established again, 0.4 mg/ml G418 was added to the medium on the selection plate. Dying G418-sensitive colonies became visible after 2 to 5 days, and corresponding clones could then be expanded from the duplicate plate (65). Deletion of the neo^r cassette was verified by Southern blot hybridization of NcoI-digested genomic DNA with a SalI-NcoI fragment as probe.

Generation of NFIX-deficient mice. Mutant ES cells were injected into C57BL/6 blastocysts, and male chimeras were bred to C57BL/6 females to transmit the disrupted allele through the germ line.

PCR genotyping. Yolk sacs of embryonic day 10.5 (E10.5) to E18.5 or 0.5-cm tail tip biopsy samples of P21 to P28 mice were shaken overnight at 56°C in 0.5 ml of Laird's buffer (200 mM NaCl, 100 mM Tris-HCl pH 8.3, 5 mM EDTA, 0.2% sodium dodecyl sulfate) containing 0.15 mg/ml proteinase K. One μl of the lysate was analyzed by PCR in a total volume of 30 μl (1 U of *Taq* DNA polymerase S [Genaxxon], 0.1 mM deoxynucleoside triphosphate mix [Fermentas], 1× PCR buffer [Genaxxon, containing 100 mM Tris-HCl pH 9.0, 500 mM KCl, 15 mM $MgCl_2$, 1.0% Triton X-100], *Nfix*-specific primer P1 at 5 pmol and P2 at 10 pmol, and *lacZ*-specific primer P3 at 15 pmol). The primer sequences were as follows: P1, 5′-GGAGCAAGTGGCAGGCGAAGCTGG-3′; P2, 5′-GGTTGATGAGAGCAACCTAC-3′; P3, 5′-CGCTTCTGGTGCCGGAAACC-3′. PCR conditions were 5 min at 94°C, 30 s at 94°C, 1 min at 60°C, and 1 min at 72°C for 40 cycles and 10 min at 72°C. PCR products were resolved on 1.5% agarose gels and visualized with ethidium bromide.

Reverse transcription-PCR (RT-PCR). Embryonic and adult RNAs from different organs were isolated with TRIzol reagent (Invitrogen), and cDNA was generated from 1 μg RNA with the SuperScript first-strand synthesis system (Invitrogen). *Nfix* transcripts were analyzed by PCR using an exon 1-specific primer (5′-GTACTCCCCGTACTGCCTCACCC-3′) and an exon 4-specific primer (5′-CTGTCACATTCCAGACCCCA-3′). PCR products were resolved on 2% agarose gels and visualized with ethidium bromide. Primers for the analysis of type II pro-collagen α1 (col2a1), osteocalcin, and tetranectin transcripts were as follows: col2a1, 5′-GCGAGAGGGGACTGAAGGGACACC-3′ (forward) and 5′-CGGGGCTGCGGATGCTCTCAAT-3′ (reverse); osteocalcin, 5′-TCTGCTCACTCTGCTGAC-3′ (forward) and 5′-GGAGCTGCTGTGACATCC-3′ (reverse); tetranectin, 5′-GGATTTTGGGGCACCTACCTG-3′ (forward) and 5′-GCATTGCTTGTCGAACCAC-3′ (reverse); hypoxanthine phosphoribosyltransferase (HPRT), 5′-CACAGGACTAGAACACCTGC-3′ (forward) and 5′-GCTGGTGAAAAGGACCTCT-3′ (reverse).

MRI methods. Mice were anesthetized and investigated using a 3.0-T magnetic resonance imaging (MRI) machine (Trio; Siemens, Erlangen, Germany). The following sequences were used: T2-weighted high-resolution fast spin echo sequences with a 512 by 512 matrix and a field of view of 100 by 100 mm. The spatial resolution in plane was 0.19 mm. The slice thickness was 0.8 mm. The dimension of one voxel was therefore 0.19 by 0.19 by 0.8 mm. We performed 15 slices in sagittal and 15 slices in transversal orientations of the whole mouse body.

Skeletal preparations and staining. Sacrificed mice were skinned, eviscerated, and fixed in 95% ethanol for 10 days. After incubation in acetone for 24 h, double staining with Alizarin red S and Alcian blue was performed (150 mg/liter Alcian blue [Sigma] in 1 volume of 70% ethanol; 50 mg/liter Alizarin red S [Sigma] in 1 volume of 95% ethanol, 1 volume of glacial acetic acid, and 17 volumes of 70% ethanol) at 37°C for 4 days. Specimens were washed for 2 h in tap water and then cleared in 1% KOH until the skeleton was clearly visible through the surrounding tissue. Following this incubation the skeleton was placed successively for 7 days into 20% glycerine–1% KOH, 50% glycerine–H_2O, 80% glycerine–H_2O, and 100% glycerine solutions.

Histological analysis. Whole brains were fixed in 4% paraformaldehyde overnight, and spines were fixed in Bouin's fixative (Sigma) for 7 days. Both tissues were then dehydrated in ethanol and embedded in paraffin. Serial sections of 4 to 10 μm were made and stained with hematoxylin and eosin (Sigma) following standard procedures. For 5-bromo-4-chloro-3-indolyl-β-D-glucuronic acid (X-Gal) staining, brains and bones were snap-frozen in OCT Tissue Tek (Reichert-Jung GmbH) and cryosectioned using a Kryo Cut 2000 cryostat (Reichert-Jung). Fourteen- to 20-μm sections were mounted on SuperFrost slides and dried for 30 min. Sections were fixed in cold 2% paraformaldehyde–0.2% glutaraldehyde and stained overnight at 37°C in X-Gal staining solution (10 mM potassium ferricyanide, 10 mM potassium ferrocyanide, 2 mM $MgCl_2$, 0.02% NP-40 in phosphate-buffered saline containing 1 mg X-Gal/ml of *N*,*N*-dimethylformamide). After X-Gal staining, slides were washed in phosphate-buffered saline, placed into tap water, and then transferred into a Nuclear Fast Red staining solution (Sigma) for 1 to 10 min. After staining, slides were dehydrated in ethanol and mounted for analysis.

3D multislice CT examination of bone structures. Mice were anesthetized and investigated on a multislice computed tomography (CT) scanner (Somatom Sensation 16; Siemens, Erlangen, Germany). Surface-rendering and volume-rendering techniques were used for three-dimensional (3D) visualization of multislice CT data to evaluate changes in bone structure in NFIX-deficient mice. Data acquisition was performed using helical multislice CT (120 kV and 120 mA; 0.6-mm collimation).

RESULTS

Targeted disruption of the *Nfix* gene. Generation of an *Nfix* null allele was achieved by homologous recombination of a replacement-type targeting vector. The targeting construct was designed to disrupt *Nfix* gene expression by an in-frame insertion of a reporter gene (*lacZ*) and a loxP-flanked PGKneo^r-pA cassette into exon 2, thereby replacing all but the first 4 bp of exon 2 and 32 bp of the following intron (Fig. 1A). Since exon 2 encodes the DNA-binding domain of the NFIX protein, deletion of this region results in a nonfunctional NFI fusion protein. The β-Gal activity of the fusion protein expressed under the endogenous *Nfix* promoter therefore reflects NFIX expression.

The targeting vector was introduced into CJ7 ES cells, and selected clones, which showed homologous recombination, were identified by Southern blot analysis (Fig. 1B). Deletion of the selection marker gene was achieved by transient Cre-mediated recombination of the two *loxP* sites and verified by Southern blot analysis (Fig. 1C). Two targeted *Nfix*^{lacZ} cell clones were injected into blastocysts to generate germ line chimeras. Male chimeras from one ES cell clone were used for matings with C57BL/6 females. Heterozygous offspring were crossed for homozygosity, and DNA from tail tip biopsy samples was taken to detect the mutated allele by PCR (data not shown) and by Southern blot analysis (Fig. 1D). To determine whether the *Nfix*^{lacZ} allele was a null allele, RT-PCR was performed. Total mRNA transcripts from brain, liver, and lung from 3-week-old littermates of each genotype were reverse transcribed, and cDNA was analyzed with *Nfix* exon 1- and exon 4-specific primers (Fig. 1E). A 622-bp fragment was amplified from wild-type and heterozygous cDNA corresponding to the full-length transcript containing exon 2 and exon 3. No such product could be amplified in tissues from homozygous animals. A smaller 147-bp PCR product was detected in ho-

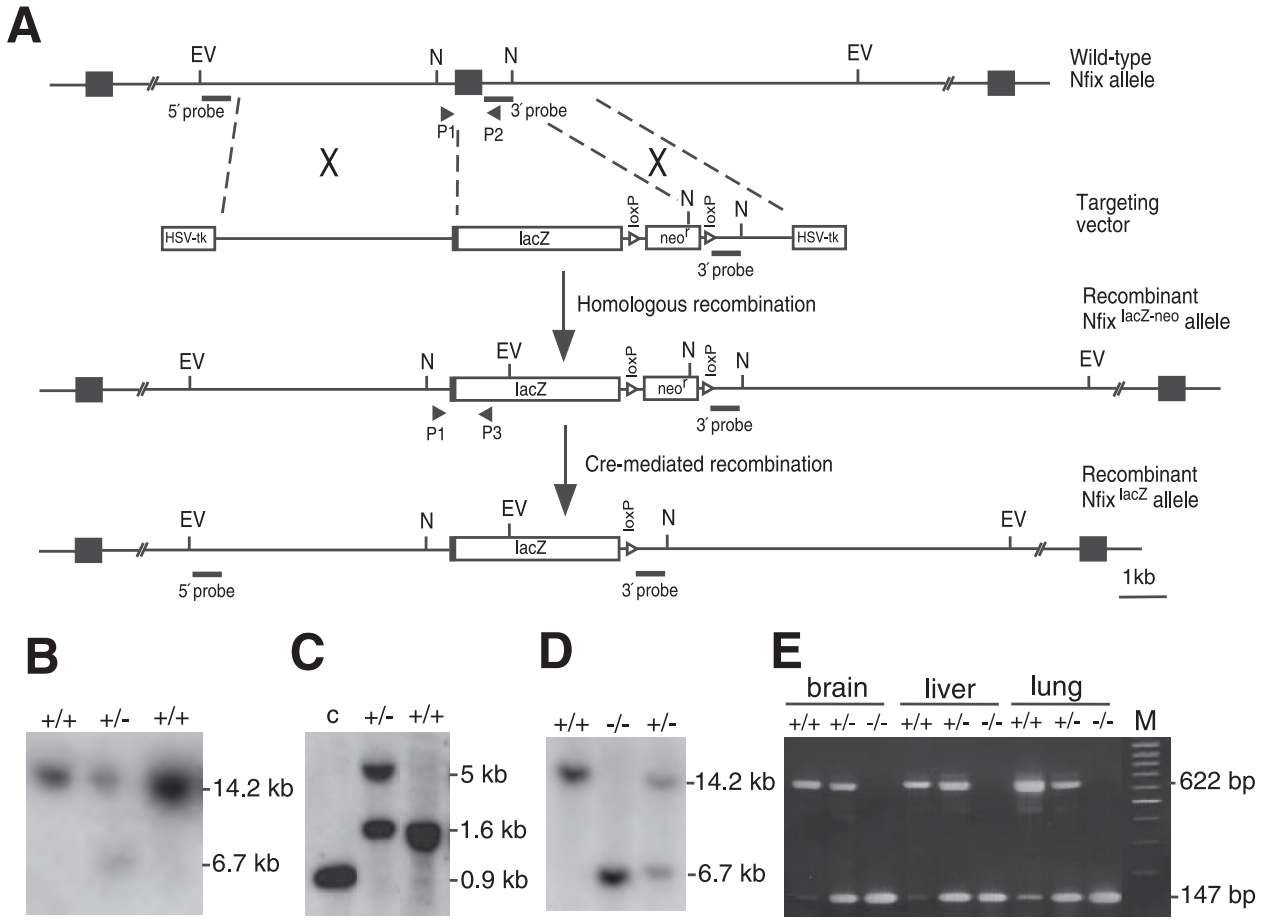

FIG. 1. Generation of an *Nfix* null allele. (A) Depicted are the first three exons (filled boxes) of the *Nfix* wild-type locus, the targeting vector, and the targeted alleles before ($Nfix^{lacZ\text{-}neor}$) and after the excision of the PGKneo^r-pA (*neo^r*) cassette by Cre-mediated recombination ($Nfix^{lacZ}$). The targeting vector contained a *lacZ* reporter gene (*lacZ*) fused into the reading frame of exon 2 (filled black box), a loxP-flanked PGKneo^r-pA (*neo^r*) selection marker (loxP sites are indicated with open triangles), and two herpes simplex virus thymidine kinase genes (*HSV-tk*). Broken lines indicate regions used for homologous recombination, and primers P1, P2, and P3 (filled triangles) for genotyping and the 5′ and 3′ probes (short bars) used for Southern blot analysis are indicated. (B) Southern blot analysis of EcoRV (EV)-digested ES cell DNA. The 5′ probe detected a 14.2-kb and a 6.7-kb band corresponding to the wild-type (+/+) and targeted (+/−) alleles, respectively. (C) Southern blot analysis for detection of the Cre-mediated neo^r-deletion. NcoI (N)-digested plasmid DNA of the targeting vector was used as a control (c), and genomic DNA from G418-sensitive $Nfix^{lacZ}$ ES cells (+/−) and genomic DNA from wild-type ES cells (+/+) was hybridized with the 3′ probe. No 0.9-kb fragment was detected in G418-sensitive cells, indicating that the *neo^r* cassette was deleted. (D) Southern blot analysis of EcoRV (EV)-digested genomic DNA from mouse tail biopsies using the 5′ probe. The sizes of the expected bands are shown for a wild-type (+/+), heterozygous (+/−), and homozygous (−/−) animal. (E) RT-PCR analysis of *Nfix* mRNA transcripts from different tissues of each genotype. Exon 1- and exon 4-specific primers amplified a 622-bp fragment corresponding to the full-length transcript and a 147-bp fragment lacking exon 2. M, 100-bp DNA marker.

mozygous and heterozygous samples and very weakly in wild-type samples. Sequencing of this smaller fragment showed that it resulted from a direct splice of exon 1 to exon 3 (data not shown). As the exon 1 to exon 3 junction is out of frame, the only possibility is that a 32-amino-acid missense polypeptide is synthesized that terminates in exon 4. It is remarkable that in tissues of $Nfix^{-/-}$ mice the exon 1 to exon 3 splice is more frequent, once the exon 2 to exon 3 splice is eliminated.

Loss of NFIX leads to postnatal lethality. From a total of 35 heterozygous matings, *Nfix* homozygous mutant animals were obtained at a normal Mendelian ratio: 95 $Nfix^{+/+}$ (31.6%), 130 $Nfix^{+/-}$ (43.3%), and 75 $Nfix^{-/-}$ (25%) mice. NFIX-deficient mice developed a dome-shaped head, were unable to fully open their eyes, and had an obvious deformation of the spine (Fig. 2A). They showed an ataxic gait and, when lifted by their tails, they drew their limbs in toward their bodies (feet-clasping posture) (9), in contrast to the full extension of limbs observed with normal littermates, indicating neurological abnormalities (Fig. 2B). With the exception of two animals that reached an age of 3 and 7 months, all other $Nfix^{-/-}$ animals died between P21 and P28 (Fig. 2C). When born, $Nfix^{-/-}$ mice were indistinguishable from their wild-type and heterozygous littermates, but by P5, daily weighing showed that $Nfix^{-/-}$ mice were unable to gain weight as efficiently as their wild-type littermates. Between P16 and P19 their weight plateaued and then progressively decreased. Shortly before death the body weight amounted to merely 60 to 70% of the weight of their normal siblings (Fig. 2D). Heterozygous mice showed a slight weight reduction but no obvious anatomical or behavioral defects (Fig. 2D).

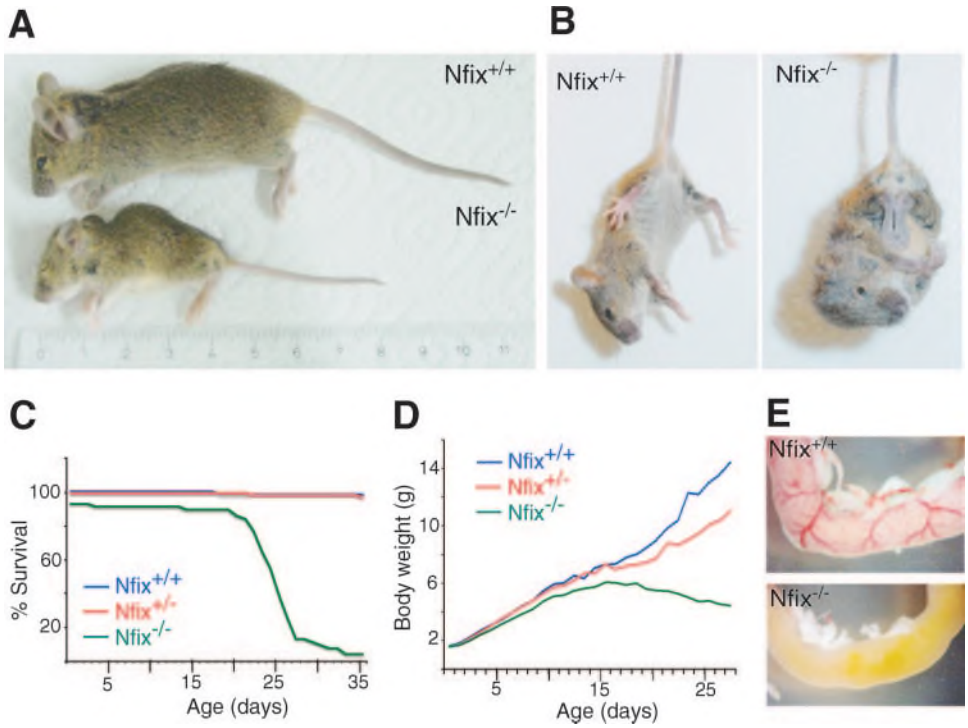

FIG. 2. Phenotype and mortality of *Nfix*$^{-/-}$ mice. (A) Wild-type (*Nfix*$^{+/+}$) and knockout (*Nfix*$^{-/-}$) mice at P24; *Nfix*$^{-/-}$ mice were 25 to 30% smaller and showed a domed head shape and a hunchback. (B) Tail suspension behavior of a wild-type (*Nfix*$^{+/+}$) and a knockout (*Nfix*$^{-/-}$) mouse. Note the characteristic nonphysiological position of the hind limbs of the *Nfix*$^{-/-}$ mouse (feet-clasping posture). Normal mice extend their limbs when lifted by their tails. (C) Mortality of *Nfix* mice. The percent survival of *Nfix*$^{-/-}$ ($n = 55$), *Nfix*$^{+/-}$ ($n = 91$), and *Nfix*$^{+/+}$ ($n = 51$) mice is plotted versus the ages of animals in days. The majority of *Nfix*$^{-/-}$ mice died between 3 and 4 weeks after birth. (D) Postnatal growth curves of *Nfix*$^{+/+}$, *Nfix*$^{+/-}$, and *Nfix*$^{-/-}$ mice. Mean body weight of mice of nine litters is plotted versus the age of animals in days. *Nfix*$^{-/-}$ mice exhibit a significant reduction in body weight after P16. (E) Dissection of the digestive tract from a wild-type (*Nfix*$^{+/+}$) and knockout (*Nfix*$^{-/-}$) mouse at P23 shows the altered appearance of the small intestine.

To further characterize the defects in *Nfix*$^{-/-}$ mice, histological examinations of inner organs were performed, but apart from a generalized reduction in size, almost all organs appeared normal. However, in all affected animals the smaller digestive tract appeared pathological, showing thinning of the intestine walls and reduced blood supply and containing a yellowish/brownish fluid (Fig. 2E). In histological preparations, myenteric neuronal innervation appeared normal, as well as the mucosa, submucosa, muscle layers, and serosa (data not shown). In addition to the intestinal anomalies, a general loss of muscle tissue was observed, but histological examination of muscle samples showed no evidence of a myopathy (data not shown). Taken together, death of *Nfix*$^{-/-}$ mice is most likely a consequence of the spectrum of neurological and intestinal problems which result in an inability to thrive.

NFIX-deficient mice develop hydrocephalus and a deformation of the spine. For further analysis, magnetic resonance imaging was performed with 3-week- and 3-month-old NFIX-deficient animals. Hydrocephalus was revealed in 3-week-old *Nfix*$^{-/-}$ mice which was characterized by dilatation of the lateral brain ventricles and the third ventricle. The fourth brain ventricle showed a normal size (Fig. 3A and B). Analysis of 3-month-old mice showed that hydrocephalus progressed with increasing age (Fig. 3C and D).

Imaging of the spine revealed a progressive skeletal pathology. The mouse spine has two physiological curvatures in the ventral axis. There is a cervico-cervical lordosis and thoracothoracical kyphosis. Angles of both vertebral bowings were measured using the Cobb method (8) in 3-week-old and 3-month-old *Nfix*$^{-/-}$ mice and compared to those of wild-type control mice. The cervical angle in 3-week-old control mice was 74.9°, and the thoracic angle was 96.4°. In NFIX-deficient mice of the same age, corresponding angles were 52.8° and 81°, respectively (Fig. 3A). At the age of 3 months, both angles in control mice became wider, measuring 88.2° for the cervical angle and 115° for the thoracic angle. In the 3-month-old *Nfix*$^{-/-}$ mouse the opposite effect was observed, as both angles became acuter and measured 41° and 52°, respectively. These changes caused severe cervico-cervical hyperlordosis and thoraco-thoracical hyperkyphosis. Because of the increased kinking of the spine, the truncal length of *Nfix*$^{-/-}$ mice appeared significantly reduced (Fig. 3C). Scoliosis, which is characterized by an abnormal lateral curvature of the spine, was also observed.

To examine the presence of primary skeletal abnormalities, whole-mount Alizarin red and Alcian blue skeletal preparations of 3-week- and 3-month-old *Nfix*$^{-/-}$ and control mice were compared. No alterations in the number of vertebral bodies, no bone deformations, and no generalized skeletal dysplasias were observed (Fig. 3E and F). Other skeletal bones, like the femur and tibia, were 25 to 30% shorter compared to wild-type animals (data not shown), which contrib-

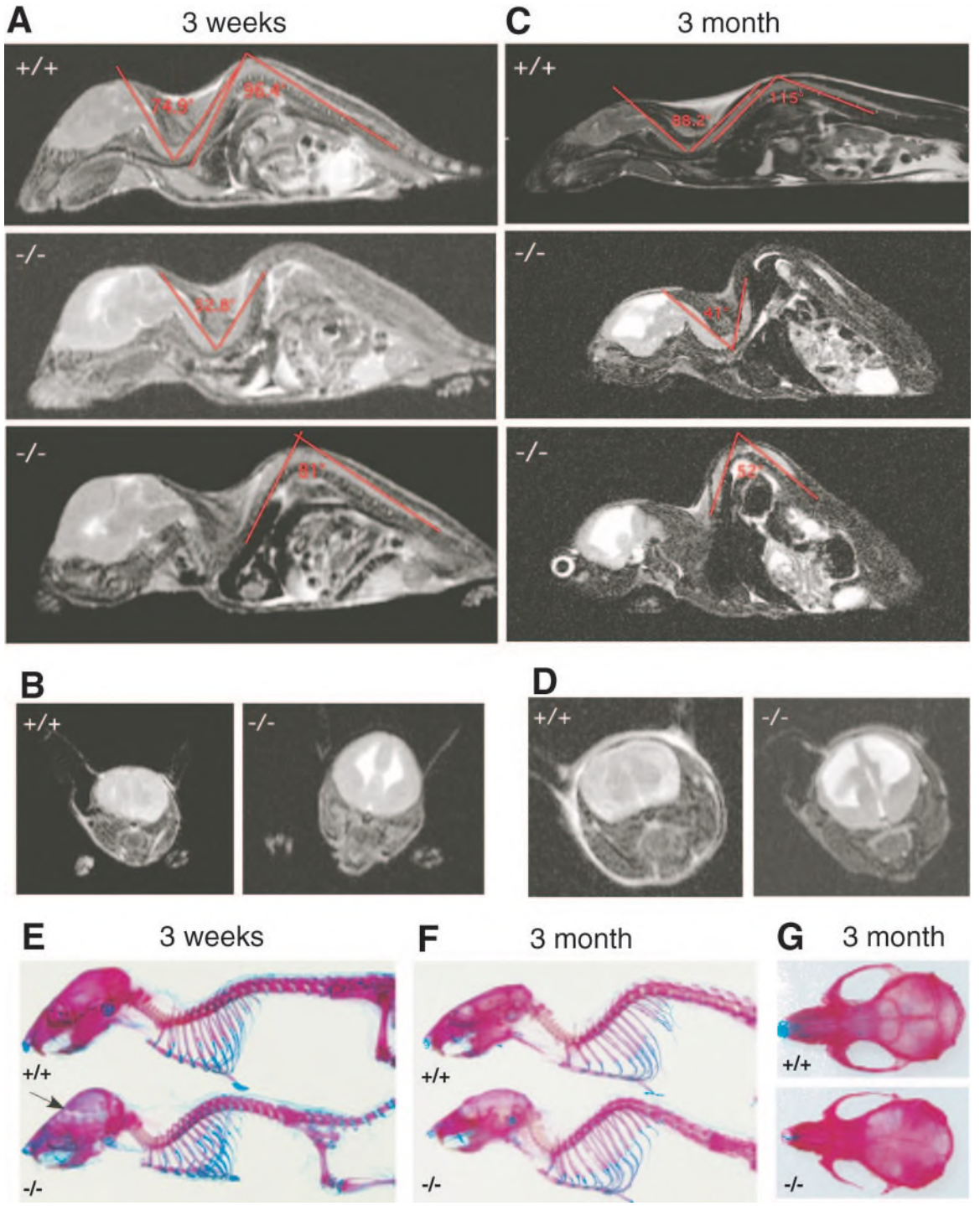

FIG. 3. MRI and skeletal analysis of *Nfix*$^{-/-}$ mice. Sagittal (A and C) and coronal (B and D) MRI analysis of 3-week-old (A and B) and 3-month-old (C and D) NFIX-deficient mice (−/−) and wild-type littermates (+/+). Angles of both vertebral bowings are depicted for the control wild-type animals in the same image, respectively (A and C, top). Note that both angles become wider during development. For the 3-week-old and 3-month-old *Nfix*$^{-/-}$ mice, the cervical and the thoracic angles are depicted in two separate pictures due to the scoliotic deformation of the spine (A and C, middle and bottom). With increasing age the cervical lordosis and the thoracic kyphosis are more pronounced. (E to G) Alizarin red- and Alcian blue-stained skeletal and skull preparations from 3-week-old (E) and 3-month-old (F and G) wild-type littermates (+/+) and NFIX-deficient mice (−/−). No congenital skeletal defect or dysplasia was evident in *Nfix*$^{-/-}$ mice (E and F). Thinning of cranial bones is marked with an arrow (E). Note the less pronounced cranial sutures in skulls of 3-month-old NFIX-deficient mice (G).

uted to the general reduction in body size of *Nfix*$^{-/-}$ mice. Alterations in cranial bones appeared to be caused by the progressive hydrocephalus and were characterized by macrocephaly, thinning of the cranial bones, and less-pronounced cranial sutures (Fig. 3E and G).

Hydrocephalus is associated with partial agenesis of the corpus callosum in *Nfix*$^{-/-}$ and *Nfix*$^{+/-}$ mice. To further characterize the hydrocephalic phenotype, serial coronal sections of brains of adult *Nfix*$^{-/-}$, *Nfix*$^{+/-}$, and wild-type mice were performed. Severe dilatation of the lateral brain ventricles and the third ventricle was noted in *Nfix*$^{-/-}$ mice compared to sections of wild-type brains. The fourth ventricle of *Nfix*$^{-/-}$ mice was not altered. In *Nfix*$^{+/-}$ mice a slight enlargement of lateral and third ventricles was also observed (Fig. 4A to F). Analysis of sagittal sections and intraventricular dye injections indicated that communication between the lateral and fourth ventricle was not inhibited, and so stenosis of the aqueduct as a possible cause for the hydrocephalus can be excluded (data not shown). Another defect observed in *Nfix*$^{-/-}$ and *Nfix*$^{+/-}$ mice was a partial agenesis of the corpus callosum. In coronal sections of rostral brain regions the callosal body was present but rather thin compared to wild-type controls (Fig. 4B and F), whereas in more-caudal regions it was completely absent in NFIX-deficient (Fig. 4G and H) and heterozygous (data not shown) animals. To analyze the expression pattern of the *Nfix* gene in the brain, we stained coronal and sagittal sections of *Nfix*$^{-/-}$ brains with X-Gal to identify the NFIX::LacZ fusion protein. Expression was detected in the hippocampal dentate gyrus, in the ependymal cell layer of the ventricular system, and in the cortex (Fig. 4I). Sagittal sections also revealed strong staining in the cerebellum (Fig. 4J).

To determine whether the observed callosal defect was already evident during development, we examined serial brain sections of E17.5 embryos. In rostral *Nfix*$^{-/-}$ brain regions the corpus callosum was present but thinner than in wild-type animals (Fig. 5A and B), whereas more caudally NFIX-deficient mice exhibited complete agenesis of the callosal body (Fig. 5G and H). A slight reduction of callosal fibers was also observed in *Nfix* heterozygous mice compared to wild-type controls (Fig. 5C to F). In addition an enlargement of lateral brain ventricles was evident at this early developmental stage in brains of *Nfix*$^{-/-}$ mice (Fig. 5G and H).

We determined by RNase protection assays the expression of a series of neuronal marker genes, including myelin basic protein, neurofilament (NF-68), and glial fibrillary acidic protein (GFAP). The analysis revealed no alterations in the expression of these genes in brains of NFIX-deficient mice compared to control mice (data not shown).

Impaired ossification in vertebral bodies of *Nfix*$^{-/-}$ mice. Besides the observed brain malformations, NFIX-deficient mice also exhibited severe skeletal abnormalities. In order to investigate the observed deformation of the vertebral column in more detail, paraffin sections of spines of 14-day-old, 23-day-old, and 7-month-old NFIX-deficient and control mice were examined (Fig. 6 and Fig. 7). Histological analysis revealed that in 14-day-old *Nfix*$^{-/-}$ mice larger amounts of cartilaginous material were present in the vertebral bodies in comparison to wild-type animals, indicating that the ossification process was delayed (data not shown). Sections of spines of 23-day-old *Nfix*$^{-/-}$ mice showed more pronounced morphological alterations. In regions of the most severe cervical and thoracic bowing, we observed that enlarged cartilaginous endplates associated with chondrocyte-like cells reached into the marrow cavity of the vertebral bodies, while control mice showed complete ossification of these structures (Fig. 6A and C). In addition, trabecular and cortical bone was thinner in bones of *Nfix*$^{-/-}$ mice than in wild-type animals (Fig. 6B and D). The intervertebral disks showed pathological alterations

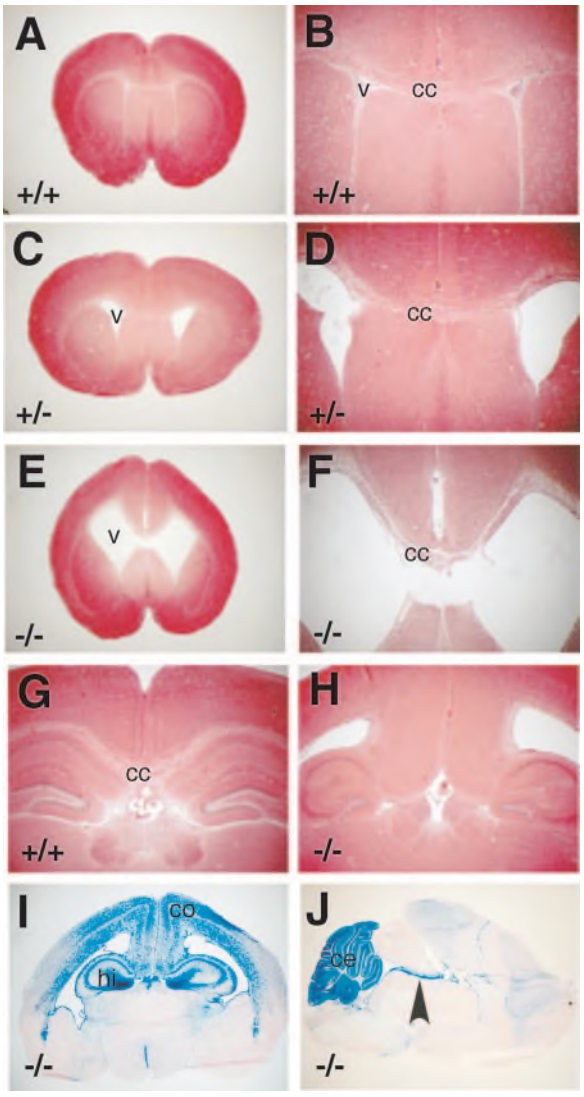

FIG. 4. Histological analysis of the brains of 23-day old mice. (A to H) Hematoxylin- and eosin-stained 6-μm coronal paraffin sections of rostral (A to F) and caudal (G and H) brain regions. Wild-type (+/+) mice revealed a normal phenotype (A and B). In heterozygous animals (+/−), the callosal body was thinner than in wild-type mice, and a slight enlargement of the ventricles was detected (C and D). In NFIX-deficient mice (−/−), severe hydrocephalus was observed and the callosal body was very thin (E and F). In caudal regions of the brain the corpus callosum was completely absent (G and H). (I and J) Histochemical staining for β-Gal activity on 20-μm coronal (I) and sagittal (J) cryosections. Highest levels of NFIX expression were detected in the hippocampus, ependymal cells (arrowhead points to the ependym of the aqueduct), and the cerebellum. Lower levels of expression were observed in the cortex. cc, corpus callosum; ce, cerebellum; co, cortex; hi, hippocampus; v, lateral brain ventricles.

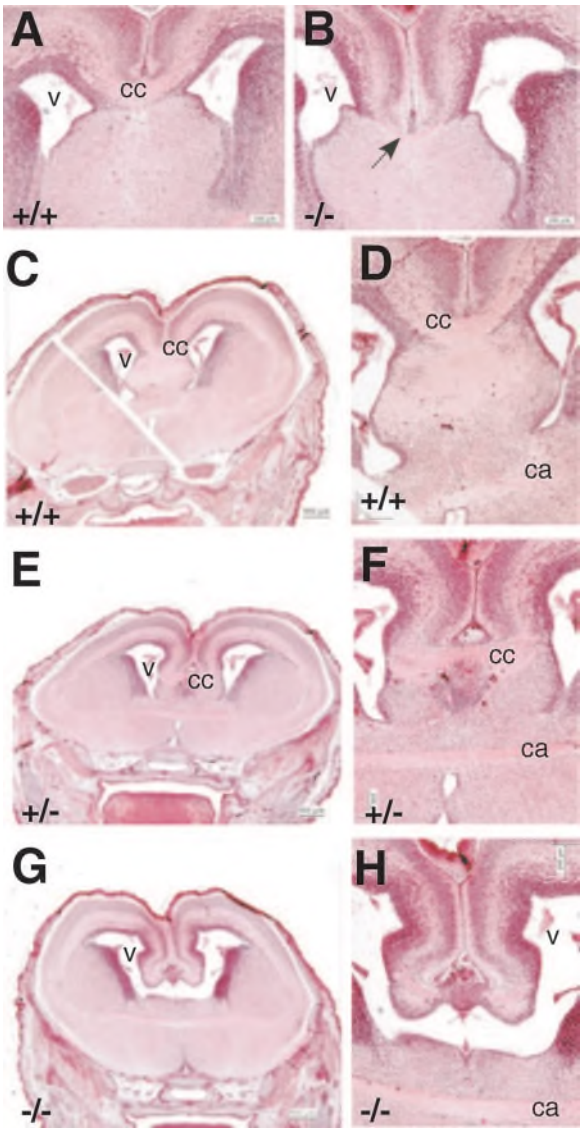

FIG. 5. Histological phenotypes of the brain at E17.5. Hematoxylin- and eosin-stained 6-μm coronal paraffin sections of the rostral brain (A and B) and in the plane of the anterior commissure (C to H). In the rostral portions of the brain a very thin callosal body is detectable in *Nfix* null mice (B, arrow) compared to wild-type mice (A). More caudally, the developing corpus callosum is readily detectable in the brains of wild-type (+/+) mice (C and D). In heterozygous animals (+/−) the callosal body is thinner (E and F), and in *Nfix* knockout mice (−/−) it is completely missing (G and H). Note that for comparison the fiber bundle of the anterior commissure is present with the same comparable diameter in the brain of either genetic background. cc, corpus callosum; ca, commissura anterior; v, lateral brain ventricles.

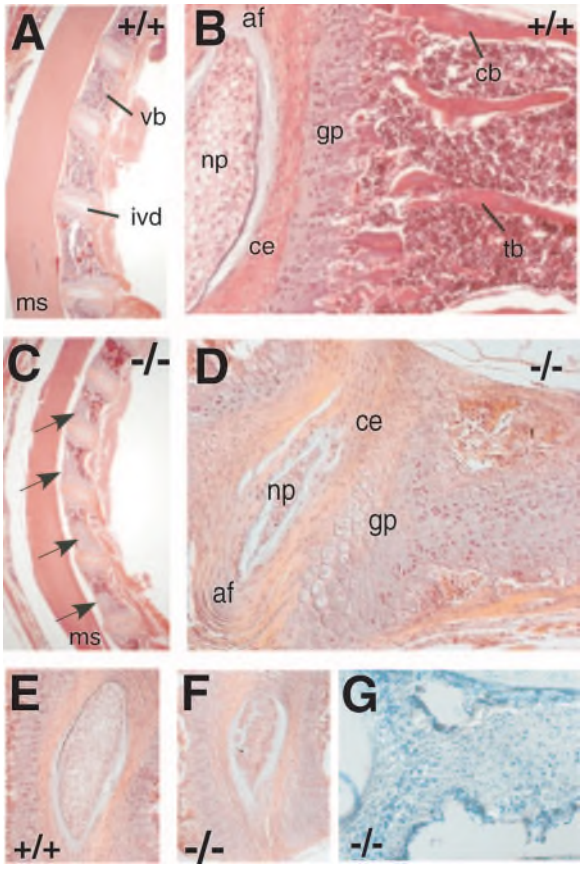

FIG. 6. Histological analysis of the vertebral columns of 23-day-old mice. Hematoxylin- and eosin-stained 6-μm sagittal paraffin sections (A to F) and X-Gal-stained 20-μm cryosections (G) are shown. (A) Sections of thoracic spine of a wild-type (+/+) mouse. (B) Closer view of the intervertebral disk and the cartilaginous endplate of a wild-type vertebral body. (C) Comparable section to that in panel A from an NFIX-deficient (−/−) mouse. Note the cartilage islands in the marrow cavity of the vertebral bodies (arrow). (D) Closer view of an intervertebral disk and a vertebral body. The amount of chondrocytes in the growth plate is increased, and the nucleus pulposus in the intervertebral disk is altered. (E and F) Intervertebral disks of $Nfix^{+/+}$ and $Nfix^{-/-}$ mice. (G) β-Gal activity in the intervertebral disk and in chondrocytes of the cartilaginous growth plate. af, annulus fibrosus; cb, cortical bone; ce, cartilaginous endplate; gp, growth plate; ivd, intervertebral disk; ms, medulla spinalis; np, nucleus pulposus; tb, trabecular bone; vb, vertebral body.

as well. They appeared irregular in shape, and the nucleus pulposus was smaller and sometimes fragmented (Fig. 6E and F). In some disks the lamellar orientation of the collagen fibers in the annulus fibrosus was also disturbed. X-Gal staining of cryosections of spines of $Nfix^{-/-}$ mice revealed *Nfix* gene expression in chondrocytes of the cartilaginous endplate and in trabecular bone (Fig. 6G). To see if the impaired ossification was overcome during maturation, the spine of the one surviving 7-month-old mouse was analyzed and compared with a wild-type mouse (Fig. 7). Vertebral bodies were completely ossified, and no remaining chondrocyte-like cells were found in the vertebral marrow in the $Nfix^{-/-}$ mouse, though cartilaginous endplates were still abnormally enlarged (Fig. 7B and D). In addition, the anterior part of the intervertebral disks seemed compressed and the nucleus pulposus exhibited degenerative changes when compared to disks of the wild-type mouse (Fig. 7).

Enlarged epiphyseal growth plates in the femurs of $Nfix^{-/-}$ mice. To analyze whether ossification was also impaired in other bones, femoral sections of 22-day-old $Nfix^{-/-}$ and wild-type mice were histologically analyzed (Fig. 8). Hematoxylin- and eosin-stained paraffin sections revealed an enlargement of the epiphyseal growth plate in $Nfix^{-/-}$ femurs compared to wild-type mice (Fig. 8A and B). This enlargement was due to

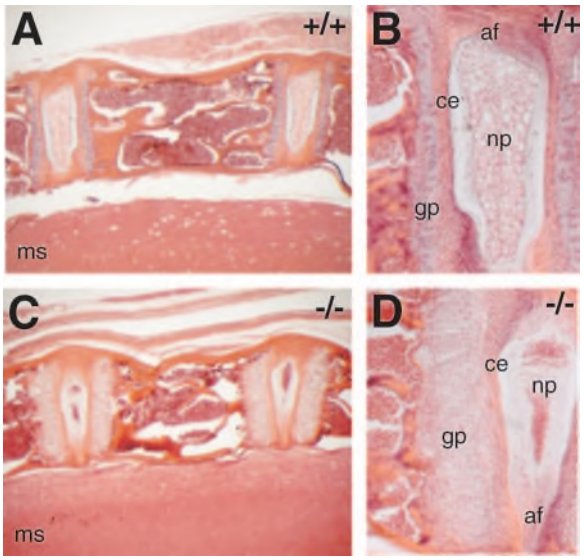

FIG. 7. Histological analysis of spines of 7-month-old mice. Hematoxylin- and eosin-stained 6-μm sagittal paraffin sections of vertebral bodies and intervertebral disks of an $Nfix^{+/+}$ mouse (A and B) and an $Nfix^{-/-}$ mouse (C and D) are shown. Growth plates of the $Nfix^{-/-}$ mouse are still enlarged, but no cartilage islands in the marrow of the vertebral bodies are observed. The nucleus pulposus of the intervertebral disk is compressed and appears degenerated. ms, medulla spinalis; np, nucleus pulposus; af, annulus fibrosus; ce, cartilaginous endplate; gp, growth plate.

an increase of the number of chondrocytes within the resting zone. In contrast, the zone of columnar proliferating chondrocytes was severely reduced and the zone of hypertrophic chondrocytes exhibited also a slight reduction (Fig. 8C and D). Trabecular bone mass was diminished, and an altered appearance of the bone marrow was evident compared to control mice (Fig. 8E and F). NFIX expression was detected in epiphyseal chondrogenic cells and also in the trabecular bone-forming cells, which corresponded to the observed defects (Fig. 8G and H). To analyze whether the impaired ossification and reduced mass of trabecular bone were associated with reduced bone density, radiographic analyses were performed. CT analysis revealed a mineralization deficiency in the hind limbs and jawbones of $Nfix^{-/-}$ mice compared to wild-type mice (Fig. 9). These findings indicate that NFIX plays an important role during endochondral ossification and mineralization.

Altered expression of tetranectin in $Nfix^{-/-}$ mice. In order to elucidate the molecular mechanism of delayed endochondral ossification and decreased mineralization in $Nfix^{-/-}$ mice, we analyzed specific skeletal marker genes. Semiquantitative RT-PCR analysis of RNA from bones of adult $Nfix^{-/-}$ and wild-type mice revealed no significant alterations in *collagen 1α1*, *collagen 2α1*, *collagen 10α1*, and *osteocalcin* gene expression (Fig. 10A and B and data not shown).

Furthermore, we analyzed the expression of the plasminogen-binding extracellular matrix protein tetranectin, because it had been postulated earlier that tetranectin plays a crucial role in mineralization during osteogenesis (68). Furthermore, tetranectin deficiency in the mouse leads to kyphosis due to an asymmetric development of growth plates and intervertebral disks (30). We detected a significant decrease in the level of

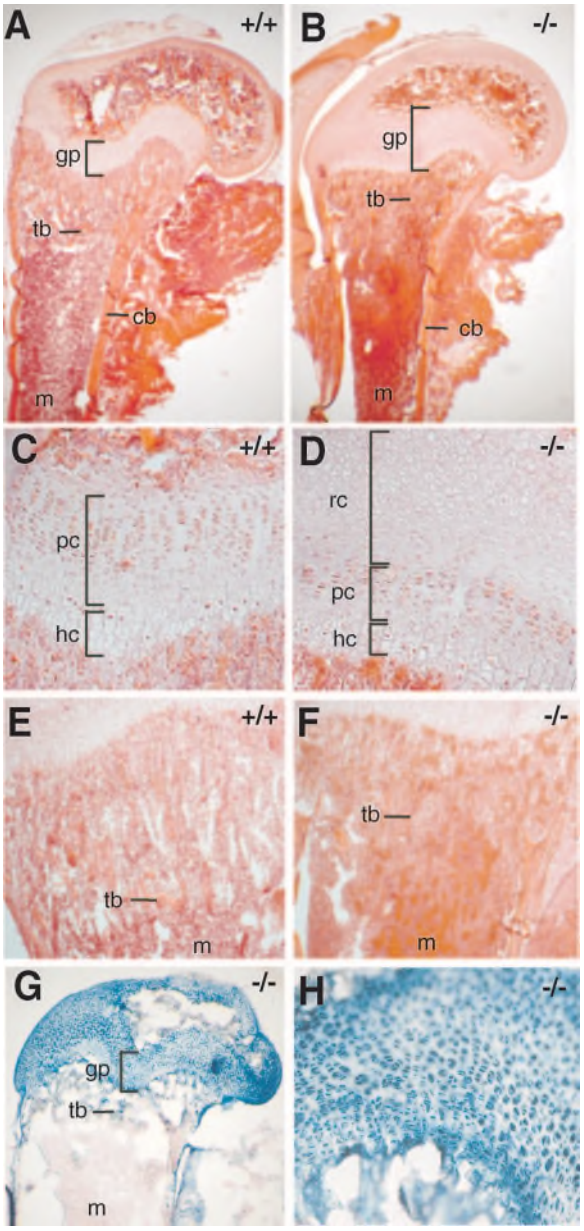

FIG. 8. Histological analysis of femurs of 22-day-old mice. Hematoxylin- and eosin-stained 6-μm longitudinal paraffin sections (A to F) and X-Gal-stained 20-μm cryosections (G and H) of NFIX-deficient (−/−) and wild-type (+/+) mice are shown. (A) Femur of an $Nfix^{+/+}$ mouse. (B) Femur of an $Nfix^{-/-}$ mouse, showing enlargement of the epiphyseal growth plate, reduction of trabecular bone, and altered bone marrow. (C and D) Epiphyseal growth plates of $Nfix^{+/+}$ and $Nfix^{-/-}$ mice. Note the increase of chondrocytes of the resting zone and reduced columnar and hypertrophic chondrocytes in panel D. (E and F) Metaphyseal regions of femurs of $Nfix^{+/+}$ and $Nfix^{-/-}$ mice. NFIX-deficient mice show reduction of trabecular bone mass and denser appearance of the bone marrow cells. (G and H) X-Gal staining of cryosections of $Nfix^{-/-}$ mice revealed NFIX expression in epiphyseal cartilaginous tissue and in trabecular bone. gp, growth plate; tb, trabecular bone; cb, cortical bone; m, marrow; pc, proliferating chondrocytes; hc, hypertrophyic chondrocytes; rc, resting chondrocytes.

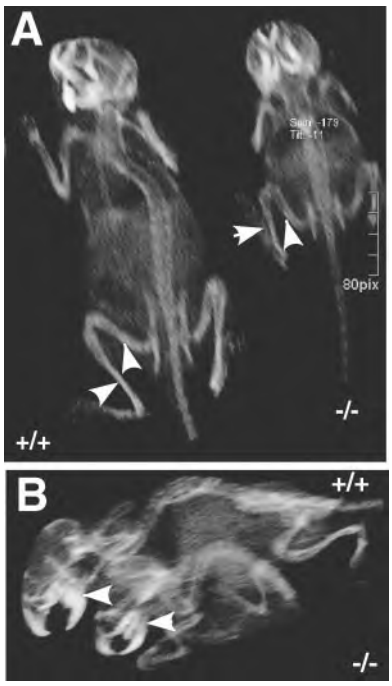

FIG. 9. 3D visualization using volume-rendering techniques of *Nfix*$^{-/-}$ and *Nfix*$^{+/+}$ 23-day-old mice. Arrowheads indicate differences in bone densities in the femur (A) and jawbone (B).

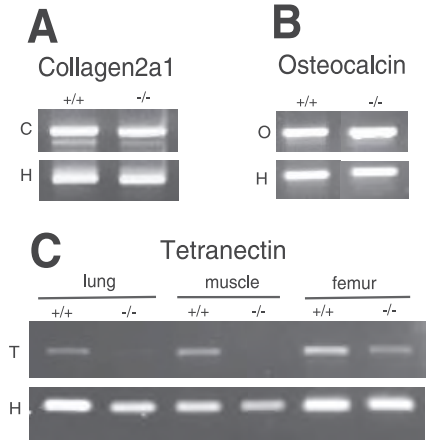

FIG. 10. Semiquantitative RT-PCR analysis of skeletal marker genes. mRNA from adult organs of wild-type (+/+) and NFIX-deficient (−/−) mice was reverse transcribed, and cDNA was analyzed by PCR with col2a1-specific (A), osteocalcin-specific (B), and tetranectin-specific (C) primers. HPRT was used as reference. C, col2a1; H, HPRT; O; osteocalcin; T, tetranectin.

tetranectin mRNA transcripts in lung, skeletal muscle, and femurs of adult *Nfix*$^{-/-}$ animals compared to wild-type tissues (Fig. 10C). These data indicate that NFIX is involved in the regulation of the activity of the tetranectin gene.

DISCUSSION

Postnatal lethality and gastrointestinal defects in *Nfix*$^{-/-}$ mice. To investigate the function of the transcription factor NFIX, we generated NFIX-deficient mice by replacing the main part of exon 2 with an in-frame insertion of the *lacZ* reporter gene (Fig. 1). *Nfix*$^{-/-}$ mice die between postnatal days 21 and 28, exhibiting brain malformations (Fig. 4 and 5) and defects in endochondral ossification (Fig. 6 to 8). Hydrocephalus is a severe brain malformation which is known to be lethal in many cases; thus, early death of NFIX-deficient mice could be a direct result of the hydrocephalus. By the time of death, *Nfix*$^{-/-}$ mice are undernourished and exhibit some pathological changes of the digestive tract (Fig. 2). As it is known that hydrocephalus is often associated with reduced appetite, it might be possible that the smaller digestive tract is a consequence of impaired food uptake. Although we observed that NFIX-deficient mice showed a visible effort to suckle and eat, calorie uptake was obviously not sufficient to survive. In addition, the kyphotic deformation of the spine might lead to difficulties in swallowing, which would also contribute to malnutrition. Tooth defects as seen in *Nfic*$^{-/-}$ mice (62) could not be found.

Alternatively, malnutrition could also be a direct cause of gastrointestinal defects. It has been shown that NFI proteins regulate muscle- and extracellular matrix-specific genes, such as the α-sarcoglycan gene in myoblasts (18), the human elastin gene (17), the mouse smooth muscle myosin heavy chain gene (73), and the OCI-5/glypican 3 gene in intestinal epithelial cells (43). Thus, it is possible that defects in intestinal connective tissue or enteric muscle function lead to the pathological appearance of the intestine in NFIX-deficient mice. The high expression levels of the *Nfix* gene in mucosa, submucosa, muscle layers, and serosa (K. Driller, S. Krück, A. Gründer, and A. E. Sippel, unpublished data) further contribute to this suggestion.

It is also known that NFI proteins activate the human intestinal type IIb Na^+-P_i cotransporter gene in the small intestinal epithelium (69) and bind to the enhancer region of the adenosine deaminase gene expressed in the intestinal epithelium at the suckling-weaning transition (47). NFI-binding sites have also been identified in the promoter region of the human sodium-dependent multivitamin transporter (19) and in the promoter region of the Na^+/H^+ exchanger gene NHE3 in intestinal epithelial cells (34). Thus, it is also possible that NFIX-deficient mice die as a result of impaired nutrient absorption due to biochemical defects in the function of intestinal cells which then would not be manifested as a gross histopathological defect. Further studies will be necessary to determine whether the malnutrition observed in *Nfix*$^{-/-}$ mice is influenced by an altered expression of any of these genes or if other factors are involved. In summary, we are presently unable to clarify whether early death of *Nfix*$^{-/-}$ mice is due more to hydrocephalus, more to the result from gastrointestinal defects, or to a combination of both.

NFIX deficiency causes hydrocephalus. Implications that NFI proteins are involved in neuronal development arose from the identification of NFI-binding sites in promoter regions of a large number of neuronal genes (32, 36, 42, 67) and also from the analysis of NFIA- and NFIB-deficient mice, which both exhibited neuronal disorders (15, 63). We showed that loss of NFIX also leads to brain malformations, including hydrocephalus and partial agenesis of the corpus callosum (Fig. 4 and 5).

It is known that hydrocephalus can be caused by several

alternative mechanisms, like overproduction of cerebrospinal fluid (CSF) (44), defects in reabsorption of CSF in the subarachnoid space (14), or impaired flow of CSF due to dysfunction of ependymal cilia or aqueductal stenosis (31). As we found no obstructions of the ventricular spaces, we presumed that CSF flow is not disturbed in *Nfix*$^{-/-}$ mice and therefore not the cause of hydrocephalus formation. Cerebrospinal fluid is mainly produced by the choroid plexus, and overproduction of CSF has been reported in mice deficient for the transcription factor E2F-5 (44) and in mice carrying a frameshift mutation in the *Hydin* gene (16). Both genes are specifically expressed in ependymal cells, and mutant mice develop severe communicating hydrocephalus. Defects in reabsorption of CSF due to impaired function of ependymal cells or disturbed extracellular matrix can also lead to the development of hydrocephalus, as seen in transgenic mice overexpressing the cytokine transforming growth factor β1 (13). Misexpression of other factors such as matrix metalloproteinases and their specific inhibitors (tissue inhibitors of matrix metalloproteinases) have also been implicated in promoting hydrocephalus formation by altering the extracellular matrix environment (70). Since the *Nfix* gene is highly expressed in ependymal cells (Fig. 4) and in the choroid plexus (K. Driller, S. Krück, A. Gründer, and A. E. Sippel, unpublished data), it might be possible that NFIX is directly or indirectly involved in the regulation of CSF production and/or reabsorption.

NFIX deficiency causes defects in corpus callosum development. As a second severe brain defect, NFIX-deficient mice showed a partial agenesis of the corpus callosum (Fig. 4 and 5). The corpus callosum is the largest fiber tract in the brain that connects the two brain hemispheres and extends from rostral to caudal brain regions. Callosal axons of the rostral part of the developing corpus callosum cross the midline at E15.5 by following so-called pioneering axons. The caudal region develops approximately 1 day later at E16.5, and callosal axons require the presence of the hippocampal commissure to cross the midline (56). In *Nfix*$^{-/-}$ mice the rostral part of the callosal body is present but rather thin, while more caudally it is completely absent, indicating that NFIX is involved in the development of both callosal regions. Given the expression of the *Nfix* gene in the cortex (Fig. 4), one could speculate that loss of NFIX results in impaired or defective outgrowth of callosal axons from cortical regions, resulting in a thin and partly absent callosal body. If axonal outgrowth is not affected, it might be that callosal axons are unable to cross the midline efficiently (rostral) or not able at all (caudal) due to defects in the pioneering axons or axons of the hippocampal commissure, respectively. In NFIA- and NFIB-deficient mice it was shown that the total absence of the corpus callosum resulted from abnormal development of midline glial populations, which was also reflected by reduced expression of the glial marker GFAP (15, 59, 63). In *Nfix*$^{-/-}$ mice histological analysis of midline glial cells did not indicate any obvious cellular defects and, also, GFAP gene expression was not altered (data not shown). Although it was postulated that NFI proteins bind to the GFAP promoter and NFIX regulates GFAP expression in astrocytes (10, 25), our data indicate that the absence of NFIX in glial cells might be compensated by other NFI family members and has no effect on GFAP expression in *Nfix*$^{-/-}$ mice. Taken together, we show that NFIX is a regulatory transcription factor crucial for correct brain formation.

Impaired bone formation in *Nfix*$^{-/-}$ mice. Currently there exists only limited knowledge about the molecular regulatory mechanisms of the complex process of bone formation. Our data indicate that NFIX is a new factor involved in this process. NFIX-deficient mice are growth retarded and exhibit a deformation of the spine (Fig. 2 and 3). Histological analysis of spines and femurs of *Nfix*$^{-/-}$ mice revealed a delay in endochondral ossification characterized by an enlarged zone of resting chondrocytes and a reduced zone of proliferating and hypertrophic chondrocytes (Fig. 6 to 8). Trabecular bone formation and calcification are significantly reduced (Fig. 9).

NFI-binding sites are often found in close proximity to binding sites of other transcription factors, such as the activator protein 1 complex (AP1) and members of the specificity protein (Sp) family. Delayed endochondral ossification was also observed in mice with a conditional knockout of the AP1 transcription factor component Fra2 (35). The ossification delay described for *Fra2*$^{-/-}$ mice was due to impaired hypertrophic chondrocyte differentiation in vertebrae and femurs and resulted in the development of kyphosis, similar to the phenotype seen in *Nfix*$^{-/-}$ mice. Fra2 is a member of the Fos family of basic leucine zipper domain proteins, which all appear to be involved in bone development (66). They function as dimers with proteins of the Jun family by forming the transcription factor AP1. The predominant AP1 dimer in vertebral development seems to be the dimer formed by Fra2 and c-Jun, because the conditional knockout of c-Jun alters intervertebral disk development, which also leads to a kyphotic deformation of the spine (5). In addition, members of the Sp family appear to be involved in bone development as well. Sp3-deficient mice exhibit defects in skeletal ossification (24). Sp1 and Sp3 are involved in the regulation of skeletal genes like collagen type X in hypertrophic chondrocytes (46) and RANKL in osteoblasts and bone marrow stromal cells (45), and Sp7 plays a role in osteoblast differentiation and bone formation (71). This raises the question whether NFI, AP-1, and Sp family members interact in transcriptional regulation of skeletal genes during bone development. In this respect it is noteworthy to mention that we had earlier observed a local connection of four Jun and four NFI genes on three different human chromosomes (1, 9, and 19) and two different mouse chromosomes (4 and 8) (54). On the other hand, an interplay among Sp1, Sp3, and NFI was already demonstrated for several basal and tissue-specific genes, such as the P2X1 gene in megakaryocytes (72), the secretin gene in neuronal cells (42), the poly(ADP-ribose) polymerase gene (40), and the α1 (I) and (III) procollagen gene in fibroblasts (1, 12). Rafty and colleagues (55) delivered the first evidence for the physical interaction of Sp1 and NFIX during regulation of the rat PDGF-A gene in vascular smooth muscle cells. That AP1-, Sp1-, and NFI-binding sites are also found in regulatory regions of skeletal genes was shown for the mouse tetranectin promoter (60). The analysis of tetranectin mRNA levels revealed altered gene expression in NFIX-deficient mice, with reduced tetranectin transcripts in lung, muscle, and bone (Fig. 10). Tetranectin is a plasminogen-binding protein with a role in tissue remodelling and a potential function in mineralization during osteogenesis (68). Tetranectin-deficient mice exhibit kyphosis due to intervertebral disk defects

(30), which indicates that tetranectin might be required for stabilizing the spine. It is assumed that the loss of tetranectin leads to the softening of the extracellular bone matrix and the intervertebral disk, which then results in spinal deformation. In accordance with that assumption, reduced tetranectin expression was also reported in mice deficient for the G-protein-coupled receptor GPR103, and these mice also developed kyphosis and reduction of trabecular bone (3). Taken together, the observed kyphotic phenotype in NFIX-deficient mice is consistent with reduced expression of tetranectin and suggests that tetranectin is a new downstream target of NFIX.

Roles of NFI proteins in development and human disorders. It is supposed that the four mammalian NFI genes arose through gene duplication and diversification from a putative NFI ancestral gene. In accordance with that, only one NFI gene (*nfi-I*) was found in the nematode *Caenorhabditis elegans* (22). The high degree of homology in gene sequence and structure is consistent with a general functional role as DNA-binding and regulatory proteins. Their specific and overlapping expression patterns indicate common, but also unique, functions for each family member. Comparison of the different knockout phenotypes of each *Nfi* gene in mouse and *C. elegans* helps to elucidate their role during development. These animal models revealed that NFI family members seem to regulate processes that occur relatively late in development, since none of the strains of knockout mice shows embryonic lethality (15, 28, 62, 63). This is surprising, given the early start of expression at E9 (*Nfia*), E9.5 (*Nfib*), E11.5 (*Nfic*), and E11.5 (*Nfix*) (11). Even loss of the putative NFI ancestral gene *nfi-I* in *C. elegans* is only lethal in adult life, though expression occurs throughout early embryogenesis (41). This indicates that during early development, NFI proteins seem to regulate downstream targets of minor importance for embryonic survival or that, in mice, other members of the *Nfi* family can compensate for the loss of one family member.

Furthermore, it is notable that three NFI-deficient strains, *Nfia*, *Nfib*, and *Nfix* null mice, exhibit similar brain defects (agenesis of the corpus callosum and hydrocephalus), which implies a common but not redundant function in brain development. This is consistent with the fact that the first organ where these three genes are expressed is the cortex in the developing forebrain. In NFIC-deficient mice no neuronal defects have been reported, although the *Nfic* gene is also expressed in the adult mouse brain (K. Driller, unpublished observation). Additionally, it has been shown that NFIC binds to the promoter of the secretin gene in neuronal cells (42) and is involved in the regulation of the GFAP gene in astrocytes (25), which raises the question whether the evolutionary distance of the *Nfic* gene in relation to the other family members is more progressed. In *nfi-I*-deficient worms, neurological defects have also been discussed to be the cause of the behavioral defects that were identified, indicating that regulation of neurological genes seems to be a conserved function of NFI family members throughout evolution.

It is striking that, besides the observed brain malformations, knockout mice for each *Nfi* gene show also very distinct defects in other organs, which is in accordance with the tissue-specific expression pattern of the four genes in different organs. Nevertheless, it is possible that related downstream targets or signaling pathways underlie these diverse defects. For example, proper lung and tooth development both depend on specifically regulated epithelial-mesenchymal interactions. This mechanism seems to be affected in $Nfib^{-/-}$ and $Nfic^{-/-}$ mice, since they show failure of lung maturation and impaired molar root formation, respectively, indicating that NFIB and NFIC contribute to epithelial-mesenchymal cross talk in the developing lung and in tooth buds. So far we have no indications that NFIX function also fits into this regulatory pattern. To gain further insight into the general function and possible redundancy of the *Nfi* gene family members, it is now possible to generate *Nfi* gene double- and triple-knockout mice. Further investigation is also needed to determine whether misexpression or mutations in NFI genes lead to human disorders. Brain defects seen in NFIA-, NFIB-, and NFIX-deficient mice resemble human malformation syndromes often associated with severe mental retardations (23). Skeletal defects such as the observed deformation of the spine in $Nfix^{-/-}$ mice appear similar to defects seen in Scheuermann's disease (7), and the multiple defects caused by NFIX deficiency resemble a new syndrome characterized by osteochondrodysplasia, associated with hydrocephalus and callosal agenesis (21). As knowledge of genetic defects in patients exhibiting these various disorders is very limited, *Nfix* might be a very interesting candidate gene to look for.

ACKNOWLEDGMENTS

We are grateful to the Knockout Core Facility of the Albert-Ludwigs-Universität Freiburg (C. Peters) for blastocyst injections and the generation of founder chimeras. Special thanks go to Gudrun Krüger for excellent technical assistance and to J. Mason for reading the manuscript.

This work was supported by grants from the Deutsche Forschungsgemeinschaft to A.E.S. (SFB 592/B5).

REFERENCES

1. **Artlett, C. M., S. J. Chen, J. Varga, and S. A. Jimenez.** 1998. Modulation of basal expression of the human alpha1(I) procollagen gene (COL1A1) by tandem NF-1/Sp1 promoter elements in normal human dermal fibroblasts. Matrix Biol. **17:**425–434.
2. **Bachurski, C. J., S. E. Kelly, S. W. Glasser, and T. A. Currier.** 1997. Nuclear factor I family members regulate the transcription of surfactant protein-C. J. Biol. Chem. **272:**32759–32766.
3. **Baribault, H., J. Danao, J. Gupte, L. Yang, B. Sun, W. Richards, and H. Tian.** 2006. The G-protein-coupled receptor GPR103 regulates bone formation. Mol. Cell. Biol. **26:**709–717.
4. **Bedford, F. K., D. Julius, and H. A. Ingraham.** 1998. Neuronal expression of the 5HT3 serotonin receptor gene requires nuclear factor 1 complexes. J. Neurosci. **18:**6186–6194.
5. **Behrens, A., J. Haigh, F. Mechta-Grigoriou, A. Nagy, M. Yaniv, and E. F. Wagner.** 2003. Impaired intervertebral disc formation in the absence of Jun. Development **130:**103–109.
6. **Borgmeyer, U., J. Nowock, and A. E. Sippel.** 1984. The TGGCA-binding protein: a eukaryotic nuclear protein recognizing a symmetrical sequence on double-stranded linear DNA. Nucleic Acids Res. **12:**4295–4311.
7. **Bradford, D. S.** 1981. Vertebral osteochondrosis (Scheuermann's kyphosis). Clin. Orthop. Relat. Res. **1981:**83–90.
8. **Bradford, D. S., J. H. Moe, F. J. Montalvo, and R. B. Winter.** 1974. Scheuermann's kyphosis and roundback deformity. Results of Milwaukee brace treatment. J. Bone Joint Surg. Am. **56:**740–758.
9. **Brunskill, E. W., L. A. Ehrman, M. T. Williams, J. Klanke, D. Hammer, T. L. Schaefer, R. Sah, G. W. Dorn II, S. S. Potter, and C. V. Vorhees.** 2005. Abnormal neurodevelopment, neurosignaling and behaviour in Npas3-deficient mice. Eur. J. Neurosci. **22:**1265–1276.
10. **Cebolla, B., and M. Vallejo.** 2006. Nuclear factor-I regulates glial fibrillary acidic protein gene expression in astrocytes differentiated from cortical precursor cells. J Neurochem. **97:**1057–1070.
11. **Chaudhry, A. Z., G. E. Lyons, and R. M. Gronostajski.** 1997. Expression patterns of the four nuclear factor I genes during mouse embryogenesis indicate a potential role in development. Dev. Dyn. **208:**313–325.
12. **Christner, P. J., T. Yufit, J. Peters, R. McGrath, R. F. Conway, and S. A.**

Jimenez. 2003. Transcriptional activation of α1(III) procollagen gene in Tsk2/+ dermal fibroblasts. Biochem. Biophys. Res. Commun. **303:**406–412.
13. **Cohen, A. R., D. W. Leifer, M. Zechel, D. P. Flaningan, J. S. Lewin, and W. D. Lust.** 1999. Characterization of a model of hydrocephalus in transgenic mice. J. Neurosurg. **91:**978–988.
14. **Crews, L., T. Wyss-Coray, and E. Masliah.** 2004. Insights into the pathogenesis of hydrocephalus from transgenic and experimental animal models. Brain Pathol. **14:**312–316.
15. **das Neves, L., C. S. Duchala, F. Tolentino-Silva, M. A. Haxhiu, C. Colmenares, W. B. Macklin, C. E. Campbell, K. G. Butz, R. M. Gronostajski, and F. Godinho.** 1999. Disruption of the murine nuclear factor I-A gene (Nfia) results in perinatal lethality, hydrocephalus, and agenesis of the corpus callosum. Proc. Natl. Acad. Sci. USA **96:**11946–11951.
16. **Davy, B. E., and M. L. Robinson.** 2003. Congenital hydrocephalus in hy3 mice is caused by a frameshift mutation in Hydin, a large novel gene. Hum. Mol. Genet. **12:**1163–1170.
17. **Degterev, A., and J. A. Foster.** 1999. The role of NF-1 factors in regulation of elastin gene transcription. Matrix Biol. **18:**295–307.
18. **Delgado-Olguin, P., H. Rosas-Vargas, F. Recillas-Targa, A. Zentella-Dehesa, M. B. de Leon, B. Cisneros, F. Salamanca, and R. Coral-Vazquez.** 2004. NFI-C2 negatively regulates alpha-sarcoglycan promoter activity in C2C12 myoblasts. Biochem. Biophys. Res. Commun. **319:**1032–1039.
19. **Dey, S., V. S. Subramanian, N. S. Chatterjee, S. A. Rubin, and H. M. Said.** 2002. Characterization of the 5′ regulatory region of the human sodium-dependent multivitamin transporter, hSMVT. Biochim. Biophys. Acta **1574:** 187–192.
20. **Djordjevic, M., and A. M. Sengupta.** 2006. Quantitative modeling and data analysis of SELEX experiments. Phys. Biol. **3:**13–28.
21. **Faye-Petersen, O. M., K. Ward, J. C. Carey, and A. S. Knisely.** 1991. Osteochondrodysplasia with rhizomelia, platyspondyly, callosal agenesis, thrombocytopenia, hydrocephalus, and hypertension. Am. J. Med. Genet. **40:**183–187.
22. **Fletcher, C. F., N. A. Jenkins, N. G. Copeland, A. Z. Chaudhry, and R. M. Gronostajski.** 1999. Exon structure of the nuclear factor I DNA-binding domain from C. elegans to mammals. Mamm. Genome **10:**390–396.
23. **Fransen, E., V. Lemmon, G. Van Camp, L. Vits, P. Coucke, and P. J. Willems.** 1995. CRASH syndrome: clinical spectrum of corpus callosum hypoplasia, retardation, adducted thumbs, spastic paraparesis and hydrocephalus due to mutations in one single gene, L1. Eur. J. Hum. Genet. **3:**273–284.
24. **Gollner, H., C. Dani, B. Phillips, S. Philipsen, and G. Suske.** 2001. Impaired ossification in mice lacking the transcription factor Sp3. Mech. Dev. **106:**77–83.
25. **Gopalan, S. M., K. M. Wilczynska, B. S. Konik, L. Bryan, and T. Kordula.** 2006. Nuclear factor-1-X regulates astrocyte-specific expression of the alpha 1-antichymotrypsin and glial fibrillary acidic protein genes. J. Biol. Chem. **281:**13126–13133.
26. **Gounari, F., R. De Francesco, J. Schmitt, P. van der Vliet, R. Cortese, and H. Stunnenberg.** 1990. Amino-terminal domain of NF1 binds to DNA as a dimer and activates adenovirus DNA replication. EMBO J. **9:**559–566.
27. **Gronostajski, R. M.** 2000. Roles of the NFI/CTF gene family in transcription and development. Gene **249:**31–45.
28. **Gründer, A., T. T. Ebel, M. Mallo, G. Schwarzkopf, T. Shimizu, A. E. Sippel, and H. Schrewe.** 2002. Nuclear factor I-B (Nfib) deficient mice have severe lung hypoplasia. Mech. Dev. **112:**69–77.
29. **Gründer, A., F. Qian, T. T. Ebel, A. Mincheva, P. Lichter, U. Kruse, and A. E. Sippel.** 2003. Genomic organization, splice products and mouse chromosomal localization of genes for transcription factor nuclear factor one. Gene **304:**171–181.
30. **Iba, K., M. E. Durkin, L. Johnsen, E. Hunziker, K. Damgaard-Pedersen, H. Zhang, E. Engvall, R. Albrechtsen, and U. M. Wewer.** 2001. Mice with a targeted deletion of the tetranectin gene exhibit a spinal deformity. Mol. Cell. Biol. **21:**7817–7825.
31. **Ibanez-Tallon, I., A. Pagenstecher, M. Fliegauf, H. Olbrich, A. Kispert, U. P. Ketelsen, A. North, N. Heintz, and H. Omran.** 2004. Dysfunction of axonemal dynein heavy chain Mdnah5 inhibits ependymal flow and reveals a novel mechanism for hydrocephalus formation. Hum. Mol. Genet. **13:**2133–2141.
32. **Inoue, T., T. Tamura, T. Furuichi, and K. Mikoshiba.** 1990. Isolation of complementary DNAs encoding a cerebellum-enriched nuclear factor I family that activates transcription from the mouse myelin basic protein promoter. J. Biol. Chem. **265:**19065–19070.
33. **Jackson, D. A., K. E. Rowader, K. Stevens, C. Jiang, P. Milos, and K. S. Zaret.** 1993. Modulation of liver-specific transcription by interactions between hepatocyte nuclear factor 3 and nuclear factor 1 binding DNA in close apposition. Mol. Cell. Biol. **13:**2401–2410.
34. **Kandasamy, R. A., and J. Orlowski.** 1996. Genomic organization and glucocorticoid transcriptional activation of the rat Na^+/H^+ exchanger Nhe3 gene. J. Biol. Chem. **271:**10551–10559.
35. **Karreth, F., A. Hoebertz, H. Scheuch, R. Eferl, and E. F. Wagner.** 2004. The AP1 transcription factor Fra2 is required for efficient cartilage development. Development **131:**5717–5725.
36. **Krohn, K., I. Rozovsky, P. Wals, B. Teter, C. P. Anderson, and C. E. Finch.** 1999. Glial fibrillary acidic protein transcription responses to transforming growth factor-β1 and interleukin-1β are mediated by a nuclear factor-1-like site in the near-upstream promoter. J. Neurochem. **72:**1353–1361.
37. **Kruse, U., F. Qian, and A. E. Sippel.** 1991. Identification of a fourth nuclear factor I gene in chicken by cDNA cloning: NFI-X. Nucleic Acids Res. **19:**6641.
38. **Kruse, U., and A. E. Sippel.** 1994. The genes for transcription factor nuclear factor I give rise to corresponding splice variants between vertebrate species. J. Mol. Biol. **238:**860–865.
39. **Kruse, U., and A. E. Sippel.** 1994. Transcription factor nuclear factor I proteins form stable homo- and heterodimers. FEBS Lett. **348:**46–50.
40. **Laniel, M. A., G. G. Poirier, and S. L. Guerin.** 2001. Nuclear factor 1 interferes with Sp1 binding through a composite element on the rat poly-(ADP-ribose) polymerase promoter to modulate its activity in vitro. J. Biol. Chem. **276:**20766–20773.
41. **Lazakovitch, E., J. M. Kalb, R. Matsumoto, K. Hirono, Y. Kohara, and R. M. Gronostajski.** 2005. nfi-1 affects behavior and life-span in C. elegans but is not essential for DNA replication or survival. BMC Dev. Biol. **5:**24.
42. **Lee, L. T., K. C. Tan-Un, M. C. Lin, and B. K. Chow.** 2005. Retinoic acid activates human secretin gene expression by Sp proteins and nuclear factor I in neuronal SH-SY5Y cells. J. Neurochem. **93:**339–350.
43. **Li, M., R. Pullano, H. L. Yang, H. K. Lee, N. G. Miyamoto, J. Filmus, and R. N. Buick.** 1997. Transcriptional regulation of OCI-5/glypican 3: elongation control of confluence-dependent induction. Oncogene **15:**1535–1544.
44. **Lindeman, G. J., L. Dagnino, S. Gaubatz, Y. Xu, R. T. Bronson, H. B. Warren, and D. M. Livingston.** 1998. A specific, nonproliferative role for E2F-5 in choroid plexus function revealed by gene targeting. Genes Dev. **12:**1092–1098.
45. **Liu, J., H. Yang, W. Liu, X. Cao, and X. Feng.** 2005. Sp1 and Sp3 regulate the basal transcription of receptor activator of nuclear factor kappa B ligand gene in osteoblasts and bone marrow stromal cells. J. Cell Biochem. **96:**716–727.
46. **Magee, C., M. Nurminskaya, L. Faverman, P. Galera, and T. F. Linsenmayer.** 2005. SP3/SP1 transcription activity regulates specific expression of collagen type X in hypertrophic chondrocytes. J. Biol. Chem. **280:** 25331–25338.
47. **Maier, E. A., M. R. Dusing, and D. A. Wiginton.** 2005. Cdx binding determines the timing of enhancer activation in postnatal duodenum. J. Biol. Chem. **280:**13195–13202.
48. **Mermod, N., E. A. O'Neill, T. J. Kelly, and R. Tjian.** 1989. The proline-rich transcriptional activator of CTF/NF-I is distinct from the replication and DNA binding domain. Cell **58:**741–753.
49. **Nehls, M., M. Messerle, A. Sirulnik, A. J. Smith, and T. Boehm.** 1994. Two large insert vectors, lambda PS and lambda KO, facilitate rapid mapping and targeted disruption of mammalian genes. BioTechniques **17:**770–775.
50. **Nowock, J., and A. E. Sippel.** 1982. Specific protein-DNA interaction at four sites flanking the chicken lysozyme gene. Cell **30:**607–615.
51. **Osada, S., S. Daimon, T. Nishihara, and M. Imagawa.** 1996. Identification of DNA binding-site preferences for nuclear factor I-A. FEBS Lett. **390:**44–46.
52. **Pham, N. L., A. Franzen, and E. G. Levin.** 2004. NF1 regulatory element functions as a repressor of tissue plasminogen activator expression. Arterioscler. Thromb. Vasc. Biol. **24:**982–987.
53. **Pirok, E. W., III, H. Li, J. R. Mensch, Jr., J. Henry, and N. B. Schwartz.** 1997. Structural and functional analysis of the chick chondroitin sulfate proteoglycan (aggrecan) promoter and enhancer region. J. Biol. Chem. **272:**11566–11574.
54. **Qian, F., U. Kruse, P. Lichter, and A. E. Sippel.** 1995. Chromosomal localization of the four genes (NFIA, B, C, and X) for the human transcription factor nuclear factor I by FISH. Genomics **28:**66–73.
55. **Rafty, L. A., F. S. Santiago, and L. M. Khachigian.** 2002. NF1/X represses PDGF A-chain transcription by interacting with Sp1 and antagonizing Sp1 occupancy of the promoter. EMBO J. **21:**334–343.
56. **Richards, L. J., C. Plachez, and T. Ren.** 2004. Mechanisms regulating the development of the corpus callosum and its agenesis in mouse and human. Clin. Genet. **66:**276–289.
57. **Robertson, E.** 1987. Embryo-derived stem cell lines, p. 71–112. *In* E. Robertson (ed.), Teratocarcinomas and embroyninc stem cells: a practical approach. IRL Press, Oxford, England.
58. **Rupp, R. A., U. Kruse, G. Multhaup, U. Gobel, K. Beyreuther, and A. E. Sippel.** 1990. Chicken NFI/TGGCA proteins are encoded by at least three independent genes: NFI-A, NFI-B and NFI-C with homologues in mammalian genomes. Nucleic Acids Res. **18:**2607–2616.
59. **Shu, T., K. G. Butz, C. Plachez, R. M. Gronostajski, and L. J. Richards.** 2003. Abnormal development of forebrain midline glia and commissural projections in Nfia knock-out mice. J. Neurosci. **23:**203–212.
60. **Sorensen, C. B., L. Berglund, and T. E. Petersen.** 1997. Cloning of the murine tetranectin gene and 5′-flanking region. Gene **201:**199–202.
61. **Spitz, F., M. Salminen, J. Demignon, A. Kahn, D. Daegelen, and P. Maire.** 1997. A combination of MEF3 and NFI proteins activates transcription in a subset of fast-twitch muscles. Mol. Cell. Biol. **17:**656–666.
62. **Steele-Perkins, G., K. G. Butz, G. E. Lyons, M. Zeichner-David, H. J. Kim,**

M. I. Cho, and R. M. Gronostajski. 2003. Essential role for NFI-C/CTF transcription-replication factor in tooth root development. Mol. Cell. Biol. **23:**1075–1084.

63. **Steele-Perkins, G., C. Plachez, K. G. Butz, G. Yang, C. J. Bachurski, S. L. Kinsman, E. D. Litwack, L. J. Richards, and R. M. Gronostajski.** 2005. The transcription factor gene *Nfib* is essential for both lung maturation and brain development. Mol. Cell. Biol. **25:**685–698.
64. **Szabo, P., J. Moitra, A. Rencendorj, G. Rakhely, T. Rauch, and I. Kiss.** 1995. Identification of a nuclear factor-I family protein-binding site in the silencer region of the cartilage matrix protein gene. J. Biol. Chem. **270:**10212–10221.
65. **Torres, R. M., and R. Kühn.** 1997. Laboratory protocols for conditional gene targeting, 1st ed. Oxford University Press, New York, NY.
66. **Wagner, E. F.** 2002. Functions of AP1 (Fos/Jun) in bone development. Ann. Rheum. Dis. **61**(Suppl. 2)**:**ii40–ii42.
67. **Wang, W., R. E. Stock, R. M. Gronostajski, Y. W. Wong, M. Schachner, and D. L. Kirkpatrick.** 2004. A role for nuclear factor I in the intrinsic control of cerebellar granule neuron gene expression. J. Biol. Chem. **279:**53491–53497.
68. **Wewer, U. M., K. Ibaraki, P. Schjorring, M. E. Durkin, M. F. Young, and R. Albrechtsen.** 1994. A potential role for tetranectin in mineralization during osteogenesis. J. Cell Biol. **127:**1767–1775.
69. **Xu, H., J. K. Uno, M. Inouye, J. F. Collins, and F. K. Ghishan.** 2005. NF1 transcriptional factor(s) is required for basal promoter activation of the human intestinal NaP_i-IIb cotransporter gene. Am. J. Physiol. Gastrointest. Liver Physiol. **288:**G175–G181.
70. **Zechel, J., H. Gohil, W. D. Lust, and A. Cohen.** 2002. Alterations in matrix metalloproteinase-9 levels and tissue inhibitor of matrix metalloproteinases-1 expression in a transforming growth factor-beta transgenic model of hydrocephalus. J. Neurosci. Res. **69:**662–668.
71. **Zhao, C., and A. Meng.** 2005. Sp1-like transcription factors are regulators of embryonic development in vertebrates. Dev. Growth Differ. **47:**201–211.
72. **Zhao, J., and S. J. Ennion.** 2006. Sp1/3 and NF-1 mediate basal transcription of the human P2X1 gene in megakaryoblastic MEG-01 cells. BMC Mol. Biol. **7:**10.
73. **Zilberman, A., V. Dave, J. Miano, E. N. Olson, and M. Periasamy.** 1998. Evolutionarily conserved promoter region containing CArG*-like elements is crucial for smooth muscle myosin heavy chain gene expression. Circ. Res. **82:**566–575.